La_3Ir_2 with Rhombohedral Er_3Ni_2-type Structure

Konrad Schäfer and Rainer Pöttgen

Institut für Anorganische und Analytische Chemie, Universität Münster, Corrensstrasse 30, 48149 Münster, Germany

Reprint requests to R. Pöttgen.
E-mail: pottgen@uni-muenster.de

Z. Naturforsch. **2014**, *69b*, 1053 – 1056
DOI: 10.5560/ZNB.2014-4146
Received July 9, 2014

La_3Ir_2 is formed upon reaction of the elements at 1273 K in a sealed silica ampoule. The structure was refined from single-crystal X-ray diffractometer data: Er_3Ni_2-type structure, $R\bar{3}$, $a = 895.26(2)$, $c = 1713.01(5)$ pm, $wR = 0.0578$, 766 F^2 values, 25 variables. The structure is composed of two simple basic building units: slightly distorted $La1@La3_6La2_2$ cubes resembling the tungsten structure and $Ir_2@La1_1La2_2La3_5$ units with an AlB_2-related coordination (298 pm Ir–Ir in the dumb-bell). Each cube is coordinated by six of the AlB_2 units. The relationship with the U_3Si_2-type structure is discussed.

Key words: Lanthanum, Iridium, Crystal Structure, Intermetallics

Introduction

Two propositions for the La-Ir phase diagram have been published [1 – 4], summarizing the work on the binary La_xIr_y phases which cover the broad range of compositions from lanthanum-rich La_4Ir to iridium-rich La_2Ir_{17} [1, 5 – 14]. Uncertainties remain for the iridium-richest phase La_2Ir_{17} as well as for La_3Ir_2. The synthetic work is certainly hampered by the drastically different melting points of lanthanum (1194 K) and iridium (2683 K) [15] along with the low chemical reactivity of iridium.

The phase of composition La_3Ir_2 was placed in the La-Ir phase diagram in the early work by Dmitrieva *et al.* [1], however, no lattice parameters had been published. In the current version of the phase diagram (Massalski compilation) [3], La_3Ir_2 is no longer listed. Instead, La_5Ir_3 with Pu_5Rh_3-type structure is reported. Nevertheless, the liquidus and solidus curves in that composition range are still uncertain.

During our recent systematic studies on rare earth (*RE*)-rich phases RE_5Ir_2X with X = Sb, Bi [16] we also studied the solid solution $La_5Ir_{2-x}Sb_{1+x}$ which exhibits the orthorhombic β-Yb_5Sb_3-type structure, space group *Pnma* with x ranging from 0 to 1.5. During the synthesis of the binary phase from a sample with the initial composition 5La : 3Ir we obtained well-shaped single crystals of the La_3Ir_2 phase initially correctly placed in the phase diagram. The synthesis and structure of this rhombohedral Er_3Ni_2-type [17] phase are reported in the present note.

Experimental

Synthesis

Starting materials for the synthesis of the La_3Ir_2 sample were lanthanum ingots (smart elements) and iridium powder (Agosi), both with stated purities better than 99.9 %. Filings of lanthanum were prepared under paraffin oil, washed with cyclohexane (both dried over sodium wire) and stored in a Schlenk tube under argon prior to use. The argon was purified with a titanium sponge (900 K), molecular sieves and silica gel. Lanthanum filings and iridium powder were subsequently mixed in the atomic ratio of 5 : 3 and finely ground under cyclohexane in a mortar. The powder was cold-pressed to a small pellet and sealed in an evacuated silica ampoule. The ampoule was placed in a muffle furnace, heated to 1023 K within 48 h, then heated to 1273 K within 96 h and kept at this temperature for another 96 h. Finally the sample was cooled to r. t. within 48 h. The resulting dark-gray sample is slightly moisture sensitive and was kept in a Schlenk tube. Direct melting reactions of the elements in an arc-melting or induction furnace did not result in La_3Ir_2.

X-Ray diffraction

The polycrystalline sample was studied by powder X-ray diffraction using the Guinier technique: imaging plate detector (Fujifilm BAS-1800), Cu$K_{\alpha1}$ radiation and α-quartz ($a = 491.30$, $c = 540.46$ pm) as an internal standard. The La_3Ir_2 lattice parameters (Table 1) were refined on the basis of the Guinier data by a least-squares refinement. The experimental pattern was compared to a calculated one [18] to ensure correct indexing. The single-crystal and powder lattice parameters agreed well.

Small block-shaped single crystals of La_3Ir_2 with conchoidal fracture were selected from the crushed annealed sample. The crystals were glued to quartz fibers using beeswax. The beeswax coating was sufficient for protection against hydrolyses. The quality of the crystals was checked

on a Buerger camera (using white Mo radiation). Intensity data were collected on a Stoe IPDS-II image plate system (graphite-monochromatized Mo radiation; $\lambda = 71.073$ pm) in oscillation mode. A numerical absorption correction was applied to the data set. Details of the data collection and the crystallographic parameters are listed in Table 1.

Table 1. Crystal data and structure refinement for La_3Ir_2, space group $R\bar{3}$, $Z = 9$.

Empirical formula	La_3Ir_2
Pearson symbol	*hR*45
Formula weight, g mol^{-1}	801.2
Unit cell dimensions	
a, pm	895.26(2)
c, pm	1713.01(5)
Cell volume, nm^3	1.1890
Calculated density, g cm^{-3}	10.07
Diffractometer type	IPDS-II
Crystal size, μm^3	$20 \times 30 \times 30$
Transm. ratio (max/min)	2.40
Detector distance, mm	60
Exposure time, min	3
ω range / increment, deg	0 – 180 / 1.0
Integr. param. (A / B / EMS)	13.2 / −3.2 / 0.013
Absorption coefficient, mm^{-1}	73.7
F(000), e	2925
θ range for data collection, deg	3 – 30
Range in *hkl*	±12, +12, ±23
Total no. reflections	1531
Independent reflections / R_{int}	766 / 0.0161
Reflections with $I > 2\,\sigma(I)$	648
Data / parameters	766 / 25
*R*1 / *wR* for $I > 2\,\sigma(I)$	0.0246 / 0.0568
*R*1 / *wR* for all data	0.0325 / 0.0578
Goodness-of-fit on F^2	1.67
Extinction coefficient	183(14)
Largest diff. peak / hole, e Å^{-3}	2.54 / −1.73

EDX data

Semiquantitative EDX analyses of the single crystal studied on the diffractometer were carried out in variable pressure mode with a Zeiss EVO® MA10 scanning electron microscope with LaB_6 and Ir as standards. The experimentally observed average composition (59±2 at.-% La : 41±2 at.-% Ir) was close to the ideal one. No impurity elements heavier than sodium (detection limit of the instrument) were detected. The standard deviation accounts for the various point analyses on the irregular block-shaped crystal.

Structure determination and refinement

Analyses of the La_3Ir_2 data set revealed a rhombohedral lattice and no further systematic extinction conditions, leading to the possible space groups *R*3, *R*32, *R*3*m*, $R\bar{3}$, and $R\bar{3}$m, of which the centrosymmetric group $R\bar{3}$ was found correct during structure refinement. The starting atomic parameters were deduced using the charge-flipping algorithm of SUPERFLIP [19], and the structure was refined with anisotropic displacement parameters for all atoms with JANA2006 [20]. Separate refinements of the occupancy parameters gave no hint for deviations from the ideal composition. All sites were fully occupied within two standard deviations. The final difference Fourier syntheses revealed no residual peaks. The refined atomic positions, displacement parameters, and interatomic distances are given in Tables 2 and 3.

Further details of the crystal structure investigation may be obtained from Fachinformationszentrum Karlsruhe,

Table 2. Atomic coordinates and anisotropic displacement parameters (pm^2) for La_3Ir_2. U_{eq} is defined as one third of the trace of the orthogonalized U_{ij} tensor.

Atom	site	*x*	*y*	*z*	U_{11}	U_{22}	U_{33}	U_{12}	U_{13}	U_{23}	U_{eq}
La1	3*a*	0	0	0	156(4)	156(4)	148(7)	78(2)	0	0	153(3)
La2	6*c*	0	0	0.20271(6)	142(3)	142(3)	145(5)	71(1)	0	0	143(2)
La3	18*f*	0.07653(8)	0.42425(8)	0.25865(4)	143(3)	149(3)	147(3)	74(2)	−4(2)	−5(2)	146(2)
Ir	18*f*	0.31468(5)	0.05762(5)	0.09739(2)	149(2)	149(2)	162(2)	59(2)	−7(1)	10(1)	160(2)

La1:	6	Ir	308.8	La3:	1	Ir	296.2	Ir:	1	La2	292.7
	2	La2	347.2		1	Ir	304.1		1	La3	296.2
	6	La3	357.4		1	Ir	308.5		1	Ir	298.4
La2:	3	Ir	292.7		1	Ir	315.9		1	La3	304.1
	3	Ir	316.3		1	Ir	335.9		1	La3	308.5
	1	La1	347.2		1	La1	357.4		1	La1	308.8
	3	La3	363.5		1	La2	363.5		1	La3	315.9
	3	La3	399.4		1	La3	379.9		1	La2	316.3
	3	La3	416.8		2	La3	386.5		1	La3	335.9
					2	La3	387.5				
					1	La2	399.4				
					1	La2	416.8				

Table 3. Interatomic distances (pm) for La_3Ir_2 calculated with the powder lattice parameters. Standard deviations are equal to or smaller than 0.2 pm. All distances of the first coordination spheres are listed.

76344 Eggenstein-Leopoldshafen, Germany (fax: +49-7247-808-666; e-mail: crysdata@fiz-karlsruhe.de, http://www.fiz-karlsruhe.de/request_for_deposited_data.html) on quoting the deposition number CSD-428057.

Discussion

The solution of the La_3Ir_2 structure revealed the Pearson code *hR*45 with the Wyckoff sequence f^2 *ca.* Inspection of the Pearson data base [21] readily indicated isotypism with Er_3Ni_2 [17]. A cutout of the large unit cell is presented in Fig. 1, and the basic building units are emphasized in Fig. 2. Each La1 atom has two La2 and six La3 neighbors in slightly distorted cubic coordination. This slab readily reminds of the tungsten structure. The iridium atoms form dumb-bells, and each of these atoms has slightly distorted trigonal-prismatic lanthanum coordination, similar to the well-known AlB_2-type structure. Each of the lanthanum-centered cubes is condensed to six of the AlB_2-related slabs. In the structurally closely related series of U_3Si_2-type intermetallics [22] (exemplarily shown for Y_3Au_2 [23]), only four AlB_2 slabs coordinate to the cubes, and these units are stacked through common square and triangular faces. Due to the six coordinating AlB_2 slabs, the condensation pattern in La_3Ir_2 is much more complex (Fig. 2).

The shortest interatomic distances in the La_3Ir_2 structure occur for La–Ir, ranging from 293 to 336 pm. The shorter ones compare well with the sum of the covalent radii for lanthanum and iridium of 295 pm [15], indicating substantial La–Ir bonding. Similar iridium-centered trigonal lanthanum prisms occur in La_4IrMg (295 – 296 pm La–Ir) [24] with cubic Gd_4RhIn-type structure [25]. The iridium dumb-bells have an Ir–Ir distance of 298 pm, significantly longer than in *fcc* iridium (272 pm) [26]. Such weak Ir–Ir interactions typically occur also in iridium-rich phosphides like $La_5Ir_{19}P_{12}$ (282 – 296 pm) [27] or $Y_7Ir_{17}P_{12}$ (274 – 286 pm) [28].

Considering the comparatively large electronegativity (Pauling scale) differences between lanthanum (1.10) and iridium (2.20), one can expect a significant charge transfer from lanthanum to iridium, resulting in highly polar La–Ir as well as Ir–Ir bonding in La_3Ir_2, similar to the isotypic platinide Ba_3Pt_2 [29]. A difference between these two phases concerns the volume contraction with respect to the constituting elements: –5.5 % for La_3Ir_2 but –24.9 % for Ba_3Pt_2. Similar high contractions also occur for the palladium-, silver-, and gold-containing representatives [30 – 34] while isoelectronic La_3Rh_2 [35] shows a value of –5.2 %. The higher electronegativity difference in Ba_3Pt_2 [29] and Ba_3Au_2 [33] accompanied by relativistic effects of Pt–Pt and Au–Au bonding account for these differences.

Finally we draw back to the La-Ir phase diagram. The present structure refinement clearly confirms La_3Ir_2, originally correctly reported by Dmitrieva *et al.* [1], although without crystallographic data at

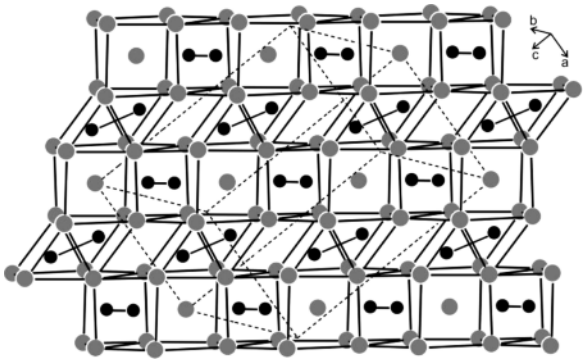

Fig. 1. Cutout of the rhombohedral La_3Ir_2 structure, space group $R\bar{3}$. Lanthanum and iridium atoms are drawn as medium grey and black circles, respectively. Approximately one layer of condensed distorted cubes (around lanthanum) and trigonal prisms (around the Ir_2 dumb-bells) is emphasized.

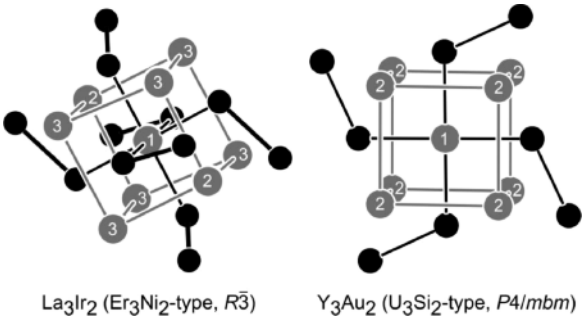

Fig. 2. Coordination of the La1 and Y1 atoms in the structures of La_3Ir_2 and Y_3Au_2 [23]. Rare earth and transition metal atoms are drawn as medium-grey and black circles, respectively. The rare earth cubes and the transition metal dumb-bells are emphasized, and the crystallographically independent rare earth sites are indicated.

that time. Our phase-analytical studies on these binaries have also shown the equiatomic phase LaIr as a by-product, most likely crystallizing with the FeB type. Further investigations on this phase are in progress.

Acknowledgement

We thank Dipl.-Ing. U. Ch. Rodewald for the intensity data collection. This work was supported by the Deutsche Forschungsgemeinschaft.

[1] V. N. Dmitrieva, V. D. Vorob'ev, L. M. Varekha, V. F. Domashev, B. A. Gusienin, *Metallofizika* **1974**, *52*, 121.
[2] W. G. Moffat, *The Handbook of Binary Phase Diagrams*, General Electric Company, Schenectady, N. Y. **1981**.
[3] T. B. Massalski (Ed.), *Binary Alloy Phase Diagrams*, ASM International, Metals Park, Ohio, **1986**.
[4] H. Okamoto, *J. Phase Equilib.* **1991**, *12*, 565.
[5] V. B. Compton, B. T. Matthias, *Acta Crystallogr.* **1959**, *12*, 651.
[6] A. E. Dwight, *Trans. Am. Soc. Met.* **1961**, *53*, 479.
[7] T. H. Geballe, B. T. Matthias, V. B. Compton, E. Corenzwit, G. W. Hull, Jr., L. D. Longinotti, *Phys. Rev.* **1965**, *137*, A119.
[8] G. L. Olcese, *J. Less-Common Met.* **1973**, *33*, 71.
[9] V. D. Vorob'ev, V. A. Mel'nikova, *Sov. Phys. Crystallogr.* **1974**, *19*, 397.
[10] D. Paccard, J. Le Roy, J.-M. Moreau, *Acta Crystallogr.* **1979**, *B35*, 1315.
[11] J. Le Roy, J.-M. Moreau, D. Paccard, E. Parthé, *Acta Crystallogr.* **1979**, *B35*, 1437.
[12] Z. Blazina, R. C. Mohanty, A. Raman, *Z. Metallkd.* **1989**, *80*, 192.
[13] C. S. Garde, J. Ray, G. Chandra, *J. Alloys Compd.* **1993**, *198*, 165.
[14] J. Prigent, J.-M. Joubert, *Intermetallics* **2011**, *19*, 295.
[15] J. Emsley, *The Elements*, Oxford University Press, Oxford **1999**.
[16] K. Schäfer, C. Schwickert, O. Niehaus, F. Winter, R. Pöttgen, *Solid State Sci.* **2014**, *35*, 66.
[17] J. M. Moreau, D. Paccard, D. Gignoux, *Acta Crystallogr. B* **1974**, *30*, 2122.
[18] K. Yvon, W. Jeitschko, E. Parthé, *J. Appl. Crystallogr.* **1977**, *10*, 73.
[19] L. Palatinus, G. Chapuis, *J. Appl. Crystallogr.* **2007**, *40*, 786.
[20] V. Petříček, M. Dušek, L. Palatinus, *Z. Kristallogr.* **2014**, *229*, 345.
[21] P. Villars, K. Cenzual, *Pearson's Crystal Data – Crystal Structure Database for Inorganic Compounds* (release 2013/14), ASM International, Materials Park, Ohio (USA) **2013**.
[22] M. Lukachuk, R. Pöttgen, *Z. Kristallogr.* **2003**, *218*, 767.
[23] P. Chai, J. D. Corbett, *Acta Crystallogr. C* **2011**, *67*, i53.
[24] U. Ch. Rodewald, S. Tuncel, B. Chevalier, R. Pöttgen, *Z. Anorg. Allg. Chem.* **2008**, *634*, 1011.
[25] R. Zaremba, U. Ch. Rodewald, R.-D. Hoffmann, R. Pöttgen, *Monatsh. Chem.* **2007**, *138*, 523.
[26] J. Donohue, *The Structures of the Elements*, Wiley, New York **1974**.
[27] U. Pfannenschmidt, U. Ch. Rodewald, R.-D. Hoffmann, R. Pöttgen, *J. Solid State Chem.* **2011**, *184*, 2731.
[28] U. Pfannenschmidt, R. Pöttgen, *Intermetallics* **2011**, *19*, 1052.
[29] A. Karpov, U. Wedig, M. Jansen, *Z. Naturforsch.* **2004**, *59b*, 1387.
[30] A. Iandelli, A. Palenzona, *J. Less-Common Met.* **1975**, *40*, 263.
[31] A. Palenzona, *J. Less-Common Met.* **1981**, *78*, P49.
[32] F. Merlo, M. L. Fornasini, *Rev. Chim. Minér.* **1984**, *21*, 273.
[33] M. L. Fornasini, F. Merlo, M. Pani, *Rev. Chim. Minér.* **1985**, *22*, 791.
[34] G. Bruzzone, M. Ferretti, F. Merlo, *J. Less-Common Met.* **1987**, *128*, 259.
[35] A. Palenzona, *J. Alloys Compd.* **1992**, *190*, 13.